

AD-A275 109

1. AGENCY U

AGE

Form Approved
OMB No. 2910-0490

4. TITLE AND SUBTITLE

Large-Scale Coronal Temperature and Density
Distributions, 1984-1992

Reprint

5. FUNDING NUMBER

PE 61102F
PR 2311
TA G3
WU 27

6. AUTHOR(S)

M. Guhathakurta*, R.R. Fisher**, R.C. Altrock

7. PERFORMING ORGANIZATION NAME(S) AND ADDRESS

Phillips Lab/GPSS
29 Randolph Road
Hanscom AFB, MA 01731-30108. PERFORMING ORGANIZATION
REPORT NUMBER

PL-TR-93-2254

S JAN 6 1994 D

9. SPONSORING MONITORING
AGENCY REPORT NUMBER

*Laboratory for Atmospheric and Space Physics, University of Colorado, Boulder, CO 80303 **NASA/Goddard Space Flight Center, Code 682, Greenbelt MD 20771

Reprinted from The Astrophysical Journal, 414: L145-L148, 1993 September 10

Approved for public release; Distribution unlimited

In this Letter we characterize the temperature and the density structure of the corona utilizing spectrophotometric observations at different heights but at the same latitude during the descending phase of cycle 21 through the ascending phase of cycle 22. The data include ground-based intensity observations of the green (Fe xiv λ 5303) and red (Fe x λ 6374) coronal forbidden lines, photospheric magnetographs from the National Solar Observatory, Kitt Peak, and synoptic maps of white-light K-coronal polarized brightness, pB , from the High Altitude Observatory. A determination of plasma temperature T can be estimated from the intensity ratio Fe x/Fe XIV (where T is inversely proportional to the ratio), since both emission lines come from ionized states of Fe, and the ratio is only weakly dependent on density. Distributions of the electron temperature from the line ratio and the polarized brightness which yields electron density of the corona during the descending and the ascending phases of solar cycles 21 and 22 are presented. These data refer to structures of the corona which are relatively large scale, having a temporal coherence of at least two or more synoptic rotation periods, such as the streamer belts, the individual helmet streamers, and the larger coronal holes. We observe that there is a large-scale organization of the inferred coronal temperature distribution that is associated with the large-scale structures in the solar magnetic fields: this organization tends to persist through most of the magnetic activity cycle. This distribution differs in spatial and temporal characterization from the traditional picture of sunspot and active region evolution over the range of sunspot cycles, which are manifestations of the small-scale, strong magnetic field regions. For example, during 1987-1990 the active region latitudes drift equatorward, whereas bright coronal features in white light and the inferred temperature structures drift poleward.

14. SUBJECT TERMS

Solar corona, Solar temperature, Solar density

15. NUMBER OF PAGES

5

16. PRICE CODE

17. SECURITY CLASSIFICATION
OF REPORT

UNCLASSIFIED

18. SECURITY CLASSIFICATION
OF THIS PAGE

UNCLASSIFIED

19. SECURITY CLASSIFICATION
OF ABSTRACT

UNCLASSIFIED

20. LIMITATION OF ABSTRACT

SAR

**Best
Available
Copy**

LARGE-SCALE CORONAL TEMPERATURE AND DENSITY DISTRIBUTIONS, 1984-1992

M. GUHATHAKURTA¹

Laboratory for Atmospheric and Space Physics, University of Colorado, Boulder, CO 80303

R. R. FISHER

NASA Goddard Space Flight Center, Code 682, Greenbelt, MD 20771

AND

R. C. ALTRICK

Phillips Laboratory (AFSC), Geophysics Directorate, National Solar Observatory/Sacramento Peak, Sunspot, NM 88349

Received 1992 November 5, accepted 1993 June 24

ABSTRACT

In this *Letter* we characterize the temperature and the density structure of the corona utilizing spectrophotometric observations at different heights but at the same latitude during the descending phase of cycle 21 through the ascending phase of cycle 22. The data include ground-based intensity observations of the green (Fe XIV $\lambda 5303$) and red (Fe X $\lambda 6374$) coronal forbidden lines, photospheric magnetographs from the National Solar Observatory, Kitt Peak, and synoptic maps of white-light K-coronal polarized brightness, pB , from the High Altitude Observatory. A determination of plasma temperature T can be estimated from the intensity ratio Fe X / Fe XIV (where T is inversely proportional to the ratio), since both emission lines come from ionized states of Fe, and the ratio is only weakly dependent on density. Distributions of the electron temperature from the line ratio and the polarized brightness which yields electron density of the corona during the descending and the ascending phases of solar cycles 21 and 22 are presented. These data refer to structures of the corona which are relatively large scale, having a temporal coherence of at least two or more synoptic rotation periods, such as the streamer belts, the individual helmet streamers, and the larger coronal holes. We observe that there is a large-scale organization of the inferred coronal temperature distribution that is associated with the large-scale structures in the solar magnetic fields; this organization tends to persist through most of the magnetic activity cycle. This distribution differs in spatial and temporal characterization from the traditional picture of sunspot and active region evolution over the range of sunspot cycles, which are manifestations of the small-scale, strong magnetic field regions. For example, during 1987-1990 the active region latitudes drift equatorward, whereas bright coronal features in white light and the inferred temperature structures drift poleward.

Subject headings: Sun: corona

1. INTRODUCTION

Knowledge of the basic conditions of temperature and density in the corona is fundamental to our understanding of the dominant physical processes that drive the corona and its solar-terrestrial connections via the interplanetary medium. However, very few accurate measurements have been made of the temperature in the inner corona. Recently, Guhathakurta et al. (1992) and Guhathakurta & Altrock (1992) determined the temperature structure of the inner corona utilizing temporal observations of the X-ray and ultraviolet intensities, the coronal green line Fe XIV, and the coronal red line Fe X during the total solar eclipse of 1988 March, and estimated average temperatures during the period 1984-1992, respectively. These studies provide a systematic method for the study of the altitudinal variation of the temperature and density as a function of the phase of the solar cycle.

The present study considers only the largest scale structure of the solar corona. The photometric data were sampled at a daily rate, and in the creation of the synoptic charts of distributions a sample size of 6° of solar latitude was used. This means that this study was band-limited to features with a spatial scale not less than 12° of latitude in width as seen at the limb, and at

least 2 days' rotation ($\sim 26^{\circ}$) in longitude. Scale sizes set by these limits are approximately 0.2 and $0.4 R_{\odot}$, respectively, and include helmet streamer, streamer belt, and larger scale coronal hole structures.

Daily observations of the solar corona are made at the National Solar Observatory at Sacramento Peak with the Photoelectric Coronal Photometer (Smartt 1982). These observations have been made in the Fe lines at 6374 and 5303 \AA which are formed at approximate temperatures of 1 and 2 MK, respectively (Altrock 1990). The $1:1$ entrance aperture is scanned daily around the limb at $1.15 R_{\odot}$.

Since 1980, the imaging K-coronameter Mark III (Fisher et al. 1984) of the High Altitude Observatory at Mauna Loa Solar Observatory in Hawaii has measured the distribution of coronal polarized brightness in white light as a function of height and azimuth around the limb of the Sun almost daily.

A set of synoptic observations of the longitudinal component of the photospheric magnetic field has been collected by the National Solar Observatory at Kitt Peak, and this set is used to provide a sense of the spatial and temporal evolution of the magnetic field of the Sun during the period of this study.

2. INTERPRETATION OF OBSERVED LINE PROFILES

In order to interpret the observed intensities in the Fe lines, we derive theoretical intensity profiles of these lines to be com-

¹ Summer faculty at NASA/GFSC, Greenbelt, MD

94-00273



pared with the observations, using the same general approach described in Guhathakurta et al. (1992), where we assume the following model corona: (1) intensity variation of the Fe lines is a function of radial distance r , along the line of sight; (2) these lines are primarily excited by collisional and radiative processes; (3) there is an ionization equilibrium distribution of ionic species; and (4) the helium abundance A_{He} is equal to 0.0851 (Allen 1973).

2.1. Intensity of the Forbidden Lines of Fe XIV and Fe X

The emissivity, E_i , of a forbidden line in the low corona is approximated by

$$E_i = D_i(T)n^\gamma \text{ (ergs cm}^{-3} \text{ s}^{-1} \text{ sr}^{-1}\text{)}, \quad (1)$$

where $i = g$ for green line intensity I_g , and $i = r$ for red line intensity I_r . Here $D_i(T)$ depends on the chemical abundances and the specific transitions as well as on the electron temperature T and to some extent on the radiation field, and n is the electron density. For forbidden coronal lines, primarily excited by collisions but for which the radiation field is also important, γ has a value between 1 and 2. The intensity observed at a height x above the limb is described by

$$I_i(x) = R_\odot \int_{-\infty}^x E_i(y) dy = 2R_\odot \int_x^\infty E_i(r) \frac{r dr}{(r^2 - x^2)^{1/2}}. \quad (2)$$

Using the same approach as in Guhathakurta et al. (1992), we can simplify the above equation and rewrite it as

$$I_i(x) = R_\odot \left(\frac{2\pi h_0}{\gamma_i} \right)^{1/2} x^{3/2} E_i(x_0) \exp \left[\frac{-\gamma_i(x - x_0)}{h_0 x x_0} \right], \quad (3)$$

where h_0 is a scale-height parameter and x_0 is some reference height.

2.2. Theoretical Emissivity of Fe XIV, Fe X

We have used Mason's (1975) excitation calculations for a dilution factor of 0.3, together with the ionization equilibrium calculations of Arnaud & Rothenflug (1985), and the abundances of Allen (1973) to calculate E_g and E_r , respectively. The quantities are (Guhathakurta et al. 1992; Guhathakurta & Altrock 1992)

$$D_g(T) = \frac{E_g}{n^{1.68}}, \quad D_r(T) = \frac{E_r}{n^{1.06}}. \quad (4)$$

3. TEMPERATURE DETERMINATION FROM EMISSION LINES

From the above analysis (eqs. [3] and [4]) we have the following equation for the intensity ratio:

$$\frac{I_r(x)}{I_g(x)} = 0.99 \left[\frac{D_g(T)}{D_r(T)} \right] n(x)^{-0.02} \approx \left[\frac{D_g(T)}{D_r(T)} \right]. \quad (5)$$

Estimated variation of the ratio D_g/D_r is presented in Figure 1, where

$$\frac{D_g(T)}{D_r(T)} = 10^{f(\log T)}. \quad (6)$$

To estimate an approximate coronal temperature distribution, we have formed the ratio $I_g(\theta, \phi)/I_r(\theta, \phi)$ (here θ is the solar latitude and ϕ is the solar longitude for each data point in the synoptic maps) using observed red and green intensities and applied equations (5) and (6). Here we have neglected the weak density variation. In general an electron density of the

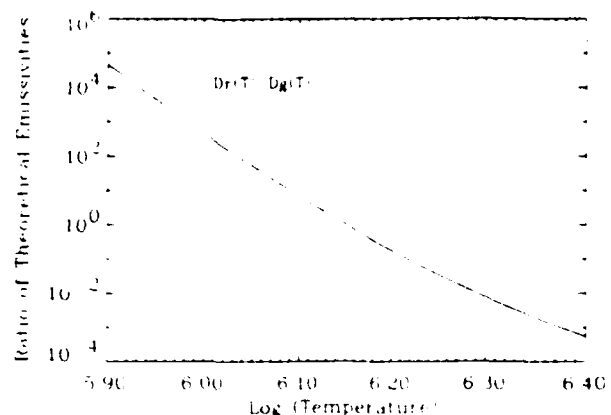


FIG. 1.—Predicted temperature dependence of the ratio $D_g(T)/D_r(T)$

order of 1×10^7 to 1×10^9 would have the effect of reducing the temperature by less than 3%. The thresholds for red and green lines are 0.1 millionths of the disk intensity B_\odot (Altrock 1993). Since the emissions from red and green lines change by almost an order of magnitude from the minimum phase to the maximum phase of the solar cycle (Guhathakurta & Altrock 1992), the relative uncertainty in the ratio of the red to the green line can change from a maximum of 75% (at the poles during minimum) to a minimum of 10% (at the equator during maximum). The uncertainty in temperature estimate can thus vary from as high as 10% during the minimum to 4% during the maximum phase of the solar cycle.

Inspection of equations (5) and (6) and Figure 1 shows that the intensity ratio is a strongly varying function of temperature T , but only a weakly varying function of density n . From Figure 1 we also notice that a dramatic change in the intensity ratio implies a small change in temperature, and therefore the precise calibration of each individual observation has a minor influence on the temperature determination. An uncertainty of one order of magnitude in the ratio of I_r/I_g leads to an error of only $\pm 12\%$ in estimating the temperature. This method offers a convenient way to establish the variation of the temperature of the inner corona over long periods of observation.

4. RESULTS

The synoptic data sets, the polarized brightness pB of the K corona, the photospheric longitudinal magnetic field, and the temperature distribution in the corona inferred from the Fe X, Fe XIV emission-line intensities are displayed (from top) in Figure 2 (Plate L11). The data are arranged so as to convey both temporal and spatial information. To eliminate high-frequency noise associated with rapid evolution and transient activity, we have added together data sets for two rotations to form an average synoptic distribution for each quantity. These averages are plotted adjacent to each other every 54 days. In Figure 2 the y-axis is solar latitude and the x-axis represents both solar longitude (in a given 54 day sample period) and time ($\approx 13.4/2 \approx 6.7$ samples per year, where it is assumed that there are 13.4 Carrington rotations in a year) as a function of time, so that the data are given as a function of both solar latitude (y-axis) and a mixed coordinate which has both spatial and temporal information (x-axis). On the scale of a single two-rotation average, the observed quantity is displayed as a function of solar latitude and longitude, assuming a latitude-invariant Carrington rotation rate. If a singular solar feature

persisted for several rotations, it would be seen in this display as a series of repetitive bright areas extending along the x-axis. This repetitive pattern would have a temporal frequency of about 6.7 per year due to the frequency of sampling the data. An example of rotational modulation can be seen in the white-light and green line records especially near the declining phase (1984) and minimum (1986) of the cycle. We have used 16 levels of color to represent white-light data ranging from 0.1 to $22 \times 10^{-8} I_{\odot}$ (disk center brightness). In this first strip of plot (top), black represents any data point below $1.38 \times 10^{-8} I_{\odot}$, the range of colors from dark to light green is $(1.38-4.13) \times 10^{-8} I_{\odot}$, beige is $(4.13-4.5) \times 10^{-8} I_{\odot}$, light blue to dark blue is $(4.5-9.63) \times 10^{-8} I_{\odot}$, purple to pink is $(9.63-13.75) \times 10^{-8} I_{\odot}$, yellow to red is $(13.75-19.25) \times 10^{-8} I_{\odot}$, and gray to white is $(19.25-22) \times 10^{-8} I_{\odot}$. The total intensity and latitude extent of the white-light corona is modulated at the frequency of the solar magnetic cycle. In the white-light plot, it is seen that as the cycle declines in 1984 toward the minimum at 1986, the white-light pB drops in amplitude (green is low pB) to a minimum and then toward the middle of 1987 begins to increase toward maximum values of pB which are displayed in pink, yellow, red near the maximum of this current cycle, 1989–1990.

The reader is reminded that there are two timescales visualized as the eye scans the x-axis. These two periodic variations result from the modulation by solar rotation and the variation associated with the solar magnetic activity cycle. Rotational modulation of the observed signal occurs at a frequency of about 6.7 cycles yr⁻¹ and magnetic activity cycle modulation occurs at the rate of ~ 1.11 cycle yr⁻¹. Solar cycle modulation of the observed quantities is easily seen in the Fe x (red line) and Fe xiv (green line) emission-line records which are plotted in the next to bottom and bottom panels of Figure 2, respectively. Since these lines are controlled largely by collisional excitation, we expect them to reflect the variation associated with approximately the square of the local electron density. The active regions are easy to pick out by inspection, since an increase in the local electron density of a factor of 3 will account for approximately an order of magnitude increase in line brightness. The solar magnetic cycle modulation of the emission-line corona by the active regions are clearly seen in these two data sets with the onset of the new cycle regions starting in mid-1988. In the red line plot, black represents any data point below $0.75 \times 10^{-6} B_{\odot}$, the range of colors from dark to light green is $(0.75-2.25) \times 10^{-6} B_{\odot}$, beige is $(2.25-3.0) \times 10^{-6} B_{\odot}$, light blue to dark blue is $(3.0-5.25) \times 10^{-6} B_{\odot}$, purple to pink is $(5.25-7.5) \times 10^{-6} B_{\odot}$, yellow to red is $(7.5-10.5) \times 10^{-6} B_{\odot}$, and gray to white is $(10.5-12) \times 10^{-6} B_{\odot}$. Similarly, in the green line plot, black represents any data point below $3.13 \times 10^{-6} B_{\odot}$, dark to light green is $(3.13-9.38) \times 10^{-6} B_{\odot}$, beige is $(9.38 \times 12.5) \times 10^{-6} B_{\odot}$, light blue to dark blue is $(12.5-21.9) \times 10^{-6} B_{\odot}$, purple to pink is $(21.9-31.13) \times 10^{-6} B_{\odot}$, yellow to red is $(31.13-43.75) \times 10^{-6} B_{\odot}$ and gray to white is $(43.75-50) \times 10^{-6} B_{\odot}$.

The photospheric magnetic field as detected by the NSO longitudinal magnetograph is plotted on the strip of data which is second from the top. In this case strong fields of opposite polarity are outlined in white/grey and black/green, while the weak fields are shaded red and blue. The 1984–1985 data have been rescaled to be consistent with the data available from 1985 to 1992, and both the rotational and the magnetic cycle modulation of the signal as a function of time are evident.

The inferred coronal temperature from the Fe x/Fe xiv ratio is shown in the middle strip of data in Figure 2. Relatively cool regions in the corona are colored green ($\sim 1.25-1.35$ MK), the intermediate regions ($\sim 1.45-1.6$ MK) are colored beige/blue, and the pink, yellow, and red regions are areas where the inferred temperature is higher (near 1.8–2.1 MK). The most prominent features of the data display are the two bands of higher temperature (pink, yellow, and red) material which are seen at relatively high latitudes on either side of the solar equator. The average temperature in these bands is found to be 1.85 ± 0.10 MK, which is about 500,000 K hotter than the average temperature (1.32 ± 0.07 MK) at the poles during solar minimum and 300,000 K hotter than the mean equatorial temperature (1.57 ± 0.11 MK) determined for the period of this study.

At the time near solar minimum, at 1986, there is relatively little variation of latitude as a function of time in the high-temperature regions. Near the maximum of the magnetic activity cycle there is a drift of the poleward boundary toward higher latitudes, first seen in the southern hemisphere, and then, about half a year later, a similar enlargement of the high-temperature region of the corona is seen to migrate toward the north polar region.

Inspection of the latitudes of the high-temperature bands yields evidence that is consistent with the location of large-scale weak-field structure in the solar magnetic field. For example, the rapid poleward spread in the high-temperature band during the 1987–1989 period of rising solar activity occurred while small-scale manifestations of activity, such as sunspots and active regions, were slowly drifting toward the equator. Further inspection of the combined photospheric magnetic field, and of the temperature, indicates that regions of higher temperature tend to be located over positions where weak photospheric fields of opposite sign are in the process of being transported toward the pole of rotation (Guhathakurta & Fisher 1992). Although not yet demonstrated by a quantitative statistical analysis, we find that prominences and bright features in the quiet corona (both related to large-scale magnetic fields) migrated toward high latitudes during 1987–1989 (Hundhausen 1993) in a manner consistent with the inferred high-temperature bands.

From the compilation of Hz synoptic charts McIntosh (1979) uses the dark disk filaments (prominences seen against the bright solar disk) in mapping the complete patterns of large-scale solar magnetic polarity. These long, persistent filaments which mark most of the patterns reveal lines of polarity reversal also known as "neutral" lines (NLs). Prominences, regions of cool, dense material at coronal heights in the vicinity of these magnetic neutral lines, are thought to be supported against solar gravity by a surrounding magnetic field structure with a spatial scale comparable to the prominence length ($\sim 0.3 R_{\odot}$; Allen 1973). The NLs that underlie the polar crown of filaments are the longest on the solar surface, interconnecting the two hemispheres. The so-called rush to the poles by the polar crown filaments is part of a process of poleward migration by a series of large-scale patterns that merge into a single feature in the year or two before maximum. This merger creates the nearly continuous chain of filaments known as the polar crown (McIntosh 1979). We observe a striking similarity in the latitudinal distributions of these polar crown filaments (McIntosh 1972; Cliver et al. 1993) during 1984–1992, and the inferred high-temperature coronal regions.

The polarized brightness distribution in Figure 2, to first order, reflects the total electron content of the corona independent of temperature. This electron content can be seen as the sum of two components, each with a distinct association with detected photospheric fields, thermal characteristics, and latitude variation with time over the cycle.

The first component is the fraction of the corona associated with the large-scale magnetic field and the boundary between weak opposite fields that is best seen near solar minimum. The white-light corona, in this case, is composed of large-scale bright persistent structures with relatively high latitudes and moderate to high density (Fig. 2). The bright features typically correspond to the centers of coronal helmet streamers (Guhathakurta et al. 1992), which are thought to have closed magnetic field lines that extend outward up to a height of about a solar radius. Enhanced inferred temperatures are seen at these latitudes.

The second component of the total variation in density of the corona over the period of study is that associated with the small-scale magnetic field and with high field strength regions of spot groups and active regions. The latitudinal variation with time is the same as that for the spot groups, drifting toward the solar equator as time advances from the maximum of the cycle. These dense coronal structures do not demonstrate elevated temperatures and to the first order seem to have a characteristic temperature which is independent of density (Guhathakurta & Fisher 1992).

In this analysis, we have used several data sets, for the purposes of comparisons, that were measured at different heights in the solar atmosphere. No effort was made to extrapolate these data to the same height. For example, the green and red line data were measured at $1.15 R_{\odot}$, the white-light data at $1.3 R_{\odot}$, and the photospheric magnetic field data at $1 R_{\odot}$. However, we find the spatial correspondence between green line bright spots and the active regions in the magnetic field data to be in close agreement, indicating that we are still observing the same features with these data sets. The latitudes of features seen on the solar disk, such as sunspots, active regions, etc., and the apparent latitudes of coronal features seen in limb observations made in white light have been studied by Hundhausen (1993), and he draws the conclusion that it is unlikely that the high-latitude coronal bright features (50° – 60°) are the projection of structures at active region latitudes (25° – 45°). Thus the inferred high-latitude, high-temperature band obtained by using emission lines, which are approximately proportional to n^4 , is not likely to be the result of projection effects of the rotation of structures at active region latitudes.

S. CONCLUSIONS

The following conclusions were drawn

1. There is an organization of the large-scale coronal temperature distribution which is associated with the large-scale structure in the solar magnetic field. Generally this organization takes the form of two zonal bands each about 20° of solar latitude in width, where the latitude boundaries are located around 50° N and 50° S.

2. These structures tend to persist through most of the solar activity cycle. Near the maximum of the sunspot cycle there was a poleward expansion of these zones while small-scale manifestations of activity such as sunspots and active regions were slowly drifting toward the equator.

3. The temperature of these zones at the reference height of $1.15 R_{\odot}$ is about 300,000 K hotter than the mean temperature inferred for the corona near the equator of the Sun and about 500,000 K hotter than the mean temperature inferred at the polar regions during solar minimum.

4. Recent analyses show that the high-temperature material of these zones tends to lie over regions where magnetograph observations indicate a change of polarity of weak large-scale magnetic fields (Guhathakurta & Fisher 1992).

5. Finally, the latitude distributions of the small-scale aspects of the solar activity as observed in sunspots and active regions, and reflected in the green and red line data and the longitudinal component of the magnetic field in Figure 2 (the so-called butterfly diagram), are significantly different from the distributions of the large-scale features as observed in white-light data and the inferred temperature structures. The latitudinal distributions of the large- and small-scale structures change in very different ways during the ascent to maximum phase (1987–1990) of the solar cycle. During this phase the active region latitudes drift equatorward, whereas bright coronal features in white light and the inferred temperature structures drift poleward.

This research was supported by a NASA summer faculty fellowship to one of us (M. G.), who would like to thank all the individuals in the SDAC group at GSFC for all the assistance with facilities and analysis that they provided. Observations at NSO/SP were obtained by Evans Facility observers under the supervision of Lou B. Gilliam, Chief Observer. K-coronometer data were supplied to us by D. Sime of the HAO. Some data reduction support was provided by Timothy W. Henry (NSO/SP) and Vic Tisone (NCAR HAO). We would like to thank J. W. Harvey (NSO/KP) for providing the synoptic magnetogram data. Finally, we would like to thank the referee for many useful suggestions.

REFERENCES

- Allen, C. W. 1973, *Astrophysical Quantities* (3d ed., London: Athlone)
- Altrock, R. C. 1990, in *Climate Impact of Solar Variability* (NASA CP-3086), 287
- 1993, private communication
- Arnaud, M., & Rothenflug, R. 1985, *A&AS*, 60, 425
- Cliver, E. W., St. Cyr, O. C., Howard, R. A., & McIntosh, P. S. 1993, in Proc. 23d Cosmic Ray Conference (Calgary), in press
- Fisher, R. R., McCabe, M., Mickey, D., Seagroves, P., & Sime, D. G. 1984, *ApJ*, 280, 873
- Guhathakurta, M., & Altrock, R. C. 1992, in *ASP Conf. Ser.* Vol. 27, *The Solar Cycle* (San Francisco: ASP), 195
- Guhathakurta, M., & Fisher, R. R. 1992, *BAAS*, 24, 4, 1254
- Guhathakurta, M., Rottman, G. J., Fisher, R. R., Orrall, F. Q., & Altrock, R. 1992, *ApJ*, 388, 633
- Hundhausen, A. J. 1993, *J. Geophys. Res.*, in press
- Mason, H. E. 1975, *MNRAS*, 170, 651
- McIntosh, P. S. 1979, UAG Report 70, World Data Center A for Solar Terrestrial Physics, Boulder
- 1992, in *ASP Conf. Ser.*, Vol. 27, *The Solar Cycle* (San Francisco: ASP), 14
- Smartt, R. N. 1982, *Proc. SPIE*, 331, 442

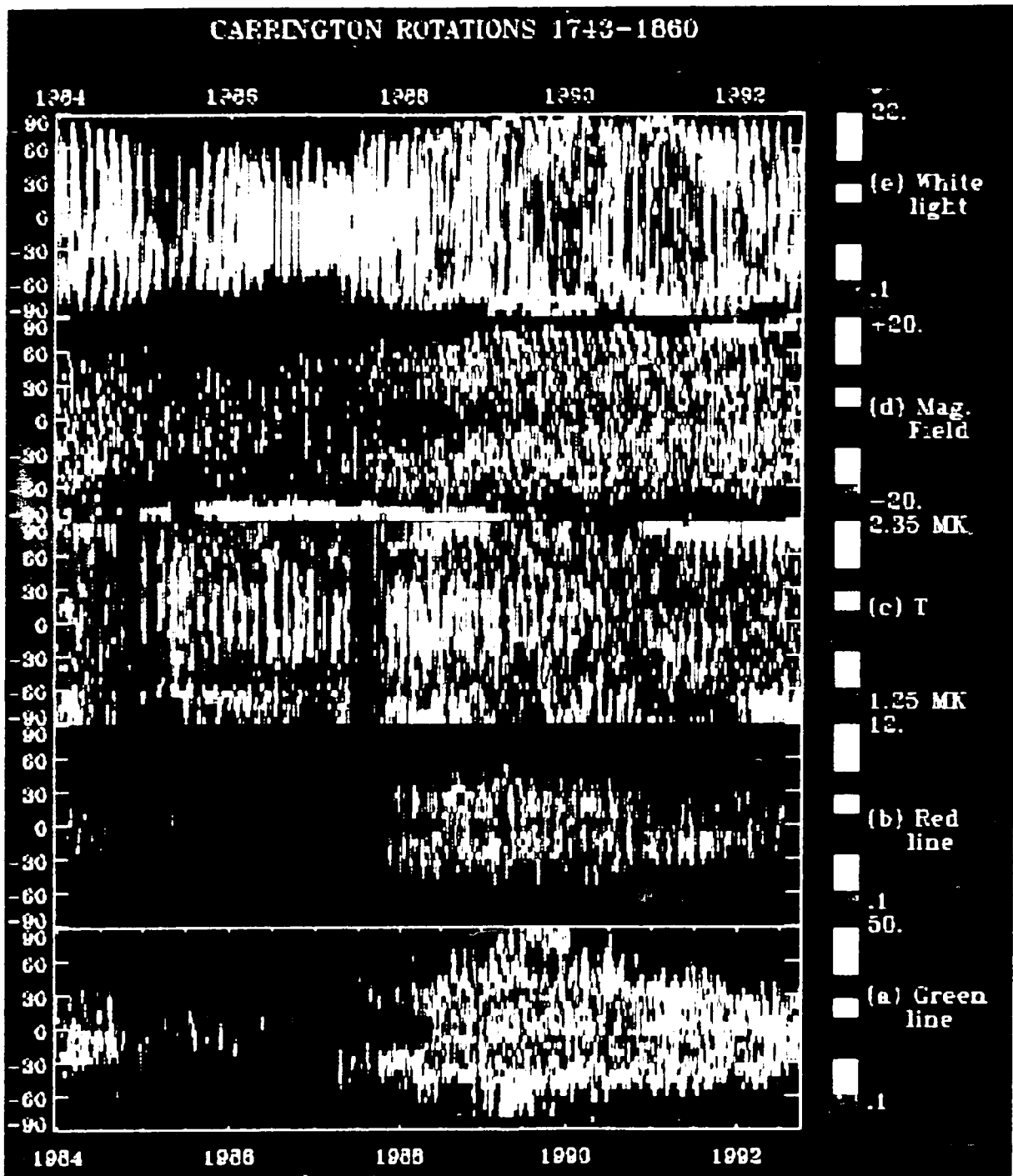


FIG. 2. Evolution of solar corona as seen at (a) green line intensity (bottom strip) in units of $10^{-4} B_{\odot}$ (total brightness of the solar disk, Allen 1973), (b) red line intensity in units of $10^{-4} B_{\odot}$, (c) the temperature estimate in MK from the line ratio (middle strip) of the inner corona at $1.15 R_{\odot}$, (d) the photospheric magnetic field from Kitt Peak, and (e) the coronal white light (top strip) at $1.1 R_{\odot}$ from Mauna Loa, Hawaii, in units of $10^{-4} I_{\odot}$ (disk center brightness of the solar disk, Allen 1973), for Carrington rotations 1743-1860 for heliographic latitudes -90° to $+90^{\circ}$. The color scale is linear and is plotted against each panel with their respective maxima and minima.